21st Australasian Fluid Mechanics Conference
Adelaide, Australia
10-13 December 2018

Singular Air Entrapment at Vertical and Horizontal Supported Jets

L. Müller[1] and H. Chanson[1]

[1]The University of Queensland
School of Civil Engineering, Brisbane 4072, Australia

Abstract

In plunging jets and at hydraulic jumps, large amounts of air bubbles are entrained at the impingement of the liquid jet and receiving body. Air is entrapped and advected into a turbulent shear layer with strong interactions between the air bubble advection process and momentum shear flow. New air-water flow measurements were repeated with identical inflow in a vertical supported jet and horizontal hydraulic jump. Detailed air-water flow measurements showed that, in both cases, the void fractions distributions followed a Gaussian profile with a pseudo-exponential decay in maximum air content. Air-water interfacial velocity profiles showed self-similar distributions, albeit there were substantial differences between horizontal hydraulic jump flow and vertical plunging jet shear layer. The transfer of momentum between impinging jet and receiving water body, as well as the buoyancy force, was affected by the flow geometry.

Introduction

In plunging jets and at hydraulic jumps, large amounts of air bubbles are entrained at the impingement of the liquid jet and receiving body [1,7,12]. Air is entrapped and advected into a turbulent shear layer with strong interactions between the air bubble advection process and the momentum shear flow [6,8,13,17]. Considering the simple case of a vertical supported jet, a free shear layer develops immediately downstream of the jet impact, and the impingement perimeter is a line source of vorticity and air bubbles. A related shear flow situation is the horizontal hydraulic jump [2,18].

In this study, new air-water flow measurements were repeated with identical inflow depth and velocity in a vertical supported jet (PJ) and a horizontal hydraulic jump (HJ). Detailed air-water flow measurements showed both similarities and differences between the two multiphase gas-liquid shear flows. The results are discussed later.

Experimental flumes, instrumentation and flow conditions

While the multiphase flow experiments were conducted in two distinct flumes, the same instrumentation and inflow conditions were used for both series of experiments. Both facilities were supplied with a constant head water reticulation system. The vertical plunging jet study was undertaken in a two-dimensional vertical supported jet flume (Fig. 1). The receiving pool was a glass tank, 1.5 m deep, 1.0 m wide and 2.5 m long. The jet nozzle delivered a 0.27 m wide, 0.012 m thick planar supported jet. The jet support was 0.35 m long, with an angle to the horizontal of 89° to prevent jet separation.

The horizontal supported jet experiment was a hydraulic jump flume, 3.20 m long and 0.5 m wide (Fig. 2). The flume bottom was made out of HDPE and the sidewalls of glass (3.20 m long panels). The flume was horizontal. The inflow was supplied through an adjustable vertical rounded gate and the downstream water level was controlled by an overshoot gate located at the downstream end of the channel.

Figure 1. Air entrainment at a vertical supported jet. Flow conditions: V_1 = 4.5 m/s, d_1 = 0.0114 m, Fr_1 = 13.5, $Re_1 = 5.14\times10^4$.

Figure 2. Air entrainment at a horizontal supported jet or hydraulic jump. Flow conditions: V_1 = 4.5 m/s, d_1 = 0.0112 m, Fr_1 = 13.5, $Re_1 = 5.14\times10^4$.

Instrumentation

The water discharge was measured with orifice and Venturi meters designed based upon British Standards and calibrated on site, with an expected error of less than 2%. The clear water depths and velocities were recorded with pointer gauges and Prandtl-Pitot tube respectively. The Prandtl-Pitot tube was a Dwyer® 166 Series tube with an outer diameter ∅ = 3.18 mm and a hemispherical total pressure tapping at the tip and eight static pressure holes equally spaced 27 mm behind the tip. Air-water flow measurements were conducted with dual-tip phase-detection probes, similar to a previous design [5,11]. The probe consisted of two needle sensors aligned in the flow direction. Each needle probe consisted of a sharpened rod (∅ = 0.25 mm) insulated except for its tip and set into a stainless steel tube acting as the second electrode. The phase-detection probe sensors were excited by an air bubble detector with a response time less than 10 μs. Further information was obtained by visual observations using photography (dSLR Pentax K3) and high-speed movies (Casio EX-10 Exilim).

Experimental flow conditions

The experiments were conducted with carefully-controlled inflow conditions. Namely identical inflow jet thickness d_1 and velocity V_1 were achieved for both vertical and horizontal supported jets, for three inflow velocities (Table 1). Herein d_1

and V_1 were recorded at the jet impingement, located at a distance $x_1 \approx 0.1$ m from the nozzle. Fr_1 and Re_1 are respectively the inflow Froude and Reynolds numbers.

Ref.	x_1 (m)	d_1 (m)	V_1 (m/s)	Fr_1	Re_1
Plunging jet	0.098	0.0076	1.79	6.56	1.37×10^4
	0.089	0.0101	2.46	7.80	2.48×10^4
	0.098	0.0114	4.50	13.45	5.14×10^4
Hydraulic jump	0.098	0.0077	1.79	6.52	1.37×10^4
	0.089	0.0101	2.46	7.80	2.48×10^4
	0.098	0.0112	4.50	13.55	5.14×10^4

Table 1. Experimental flow conditions for air-water gas-liquid measurements at vertical and horizontal supported jets.

Results. (1) Basic air-water flow patterns

At a hydraulic jump and a plunging jet, air bubbles are entrained at the flow discontinuity between the impinging jet and the downstream water body [7]. The impingement point is a flow singularity, generating vorticity and air bubble entrainment [4,7]. Downstream of the impingement point, two substantially different flow regions can be distinguished. The momentum shear layer, where viscous forces are dominant, and an outer region, where the movement of the air bubbles is mainly buoyancy-driven [4,7,21].

Advection Speed of Vortices

In the developing shear layer, large-scale coherent structures are advected within the mixing layer. The strong turbulent shear and bubble trapping lead to break-up and coalescence of air bubbles [9]. The advection speed U_{eddy} of the large-scale vortices was recorded between their formation at the impingement point and the downstream region. The data were determined manually based upon a frame-by-frame analysis of clearly visible vortices. The data yielded a symmetric Gaussian distribution of the advection speed around its mean value, for all inflow velocities in both plunging jet and hydraulic jump. The dimensionless average advection speed of vortices U_{eddy}/V_1 was 0.16 in the plunging jet, and about 0.21 in the hydraulic jump, as summarised in Table 2.

	Fr_1	Re_1	U_{eddy}/V_1	
V_1 [m/s]	PJ & HJ	PJ & HJ	PJ	HJ
1.79	6.5	1.37×10^4	0.16	---
2.46	7.8	2.48×10^4	0.15	0.23
4.50	13.5	5.14×10^4	0.17	0.20

Table 2 Average advection speed of vortices: comparison between plunging jet and hydraulic jump.

Impingement Perimeter Analysis

The characteristics of the water surface in the plunging jet and the roller toe in the hydraulic jump were analysed based on sideview observations, with a focus on the position and fluctuations of the impingement perimeter. High-speed movies were recorded with a Casio EX-10 camera at 120 fps with a resolution of 640x480 pixels. A total of 10 seconds were analysed with an entropy filter in MATLAB. After binarisation of the image, the instantaneous positions of the impingement perimeter was determined every 8.33 ms (Fig. 3).

The data showed that the impingement point fluctuated with different frequencies and amplitudes, depending upon the inflow conditions and geometry. The impingement properties between plunging jet and hydraulic jump showed substantial differences under the same inflow conditions (V_1 and d_1). The impingement perimeter fluctuation frequencies were generally higher for the plunging jet than for the hydraulic jump. Different frequencies were observed for all three inflow velocities in the plunging jet, whereas they were about the same in the hydraulic jump for all three inflow velocities (Table 3). The amplitudes of the fluctuations however, were about 3 to 9 times larger in the hydraulic jump than in the plunging jet (Table 3).

	Fluctuation frequency f [Hz]		Maximum amplitude Δ [mm]		Strouhal number $f\times d_1/V_1$	
V_1 (m/s)	PJ	HJ	PJ	HJ	PJ	HJ
1.79	5.1	2.7	2	30-40	0.022	0.012
2.46	2.2	2.7	3	40	0.009	0.011
4.50	1.7	2.7	10	60-80	0.004	0.007

Table 3 Summary of fluctuation frequencies and maximum amplitudes of the impingement perimeter fluctuations in plunging jet and hydraulic jump.

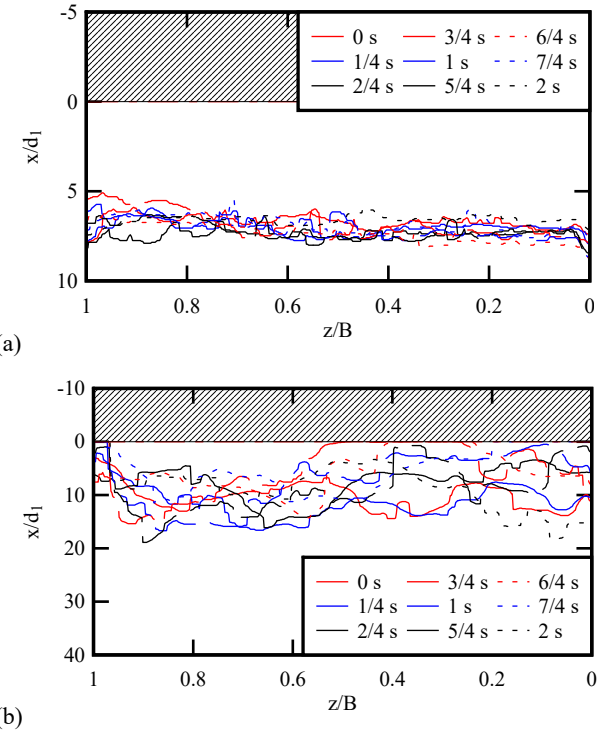

Figure 3. Instantaneous impingement perimeter every 0.25 seconds for V_1 = 4.50 m/s in the plunging jet (a) and the hydraulic jump (b) tracked by MATLAB analysis. The theoretical impingement point was at x_1/d_1 = 8.6 for the plunging jet and at x_1/d_1 = 8.7 for the hydraulic jump.

The characteristic wavelength of the impingement perimeter fluctuations was analysed with a spectral analysis (FFT). The analysis yielded a characteristic wavelength for the two smaller velocities in the plunging jet equal to about 30 mm, matching the channel width divided by the number of ridges observed in the free jet. For V_1 = 4.50 m/s, no characteristic wavelength could be found, as there were no ridges in the free jet. In the hydraulic jump, the analysis was difficult, as both the FFT spectral analysis and visual observations did not yield any characteristic wave length of the impingement perimeter.

Results. (2) Air-water flow properties

Void Fraction

In the plunging jet, the time-averaged void fraction distributions followed a quasi-Gaussian shape. At a given distance $x-x_1$ from impingement, the air content increased with increasing distance y from the jet support, reaching its maximum in the advective air diffusion layer. The void fraction then decreased with further increase in transverse distance y, reaching negligible values in the outer region where the movement of the bubbles was buoyancy driven. The maximum void fraction decreased with increasing distance from the impingement point ($x-x_1$), for a given inflow velocity. The void fraction distributions in the hydraulic jump showed a similar behaviour in the advective diffusion layer. At a given distance $x-x_1$, the void fraction increased with increasing distance from the bottom, reaching also a local maximum in the advective diffusion layer. Above, it decreased, reaching a local void fraction minimum C* at a characteristic elevation y*, corresponding to the boundary between the turbulent shear region and the upper recirculation region. For $y > y^*$, the void fractions in the hydraulic jump increased towards unity for all cross-sections, evidence of free-surface interfacial aeration in the upper flow region of the jump roller.

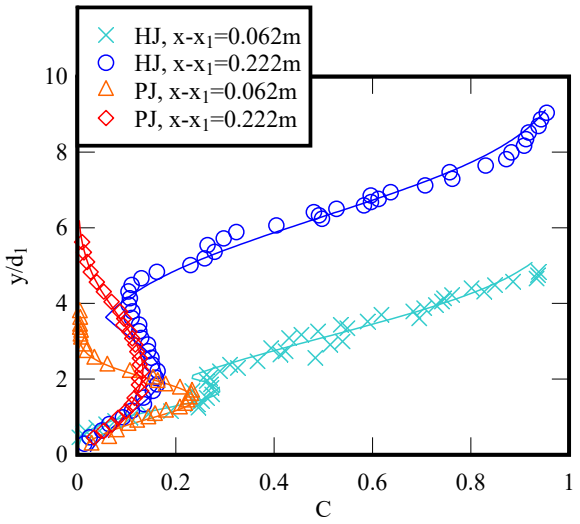

Figure 4. Void fractions distribution in plunging jet and hydraulic jump at two locations from the impingement point – comparison with analytical solutions (solid lines). (V_1 = 4.50 m/s, Fr_1 = 13.5, Re_1 = 5.14×10^4).

The plunging jet void fraction data were compared to an analytical solution, derived from the continuity equation of air in a small control volume [4]. The theory is based upon the assumption of a constant turbulent diffusivity and an advection velocity independent of x. In the hydraulic jump, two analytical solutions of the void fraction were proposed: for the turbulent shear layer ($y < y^*$) and the upper flow region ($y > y^*$). The theoretical solution for the turbulent shear layer was based on the continuity of air [9,19] assuming a constant diffusivity and steady flow conditions. The void fraction in the recirculation was equally derived from the continuity equation, assuming an analogy to a water jet discharging into air [3,9,19]. Experimental results are compared to theoretical solutions in Figure 4, highlighting the differences in void fraction between hydraulic jump and plunging jet in the outer region.

The data in terms of maximum void fraction C_{max} in the shear layer and the corresponding location Y_{Cmax} showed a good agreement with literature. Namely, the maximum void fraction decayed exponentially with increasing distance from the impingement point, and the dimensionless transverse position of the maximum void fraction Y_{Cmax}/d_1 showed a linear increasing trend with increasing $(x-x_1)/d_1$.

Velocity Profiles

In the plunging jet, the velocity field corresponded to a free-shear layer, characterised by a positive velocity next to the jet support and a negative velocity in the upward buoyancy region. In the present study, no boundary layer could be detected next to the support. In the hydraulic jump, the velocity field presented similarities with a wall jet [14,16], with an increase in velocity in the boundary layer close to the channel bed until reaching its maximum in the turbulent shear layer. The hydraulic jump velocity data showed a markedly negative velocity the upper flow region, associated with the strong recirculation motion. Experimental measurements are reported in Figure 5. In Figure 5, the velocity data in the plunging jet are compared to an analytical solution of the free shear layer [15,20], while the hydraulic jump velocity data are compared to the wall jet solution [9,10,14).

Despite some scatter, the transverse position of the maximum velocity V_{max} was approximately constant independently of $(x-x_1)/d_1$ for both plunging jet and hydraulic jump. The maximum velocity was generally observed at $Y_{Vmax}/d_1 \approx 0.5$, corresponding to the limit between the boundary layer and the turbulent shear region.

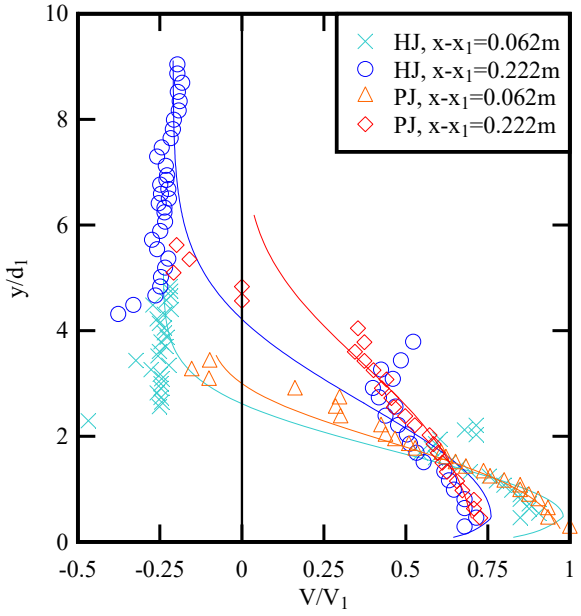

Figure 5. Velocity distribution in plunging jet and hydraulic jump at two locations from the impingement point – comparison with analytical solutions (solid lines). (V_1 = 4.50 m/s, Fr_1 = 13.5, Re_1 = 5.14×10^4).

Conclusion

Key physical differences between horizontal (hydraulic jump) and vertical supported jets (plunging jet) were analysed based upon air-water flow experiments, carried out under identical inflow conditions in terms of inflow depth and inflow velocity. Three inflow velocities were tested systematically: V_1 = 1.79 m/s, 2.46 m/s and 4.50 m/s. Visually, the

observations showed a key difference in the outer region: a buoyancy-drive flow in the plunging jet with negligible void fraction, versus a strong recirculation motion with interfacial aeration in the hydraulic jump. An analysis of the impingement conditions showed generally higher impingement perimeter fluctuation frequencies and much smaller fluctuation amplitudes in the plunging jet than in the hydraulic jump, for identical inflow conditions.

Both flow conditions yielded intense local singular air entrainment and the hydraulic jump could be described as a limiting case of a horizontal plunging jet [4]. Yet the experiments showed significant differences. These were primarily the velocity distributions, the direction of buoyancy forces and the interfacial aeration in the hydraulic jump. The velocity distributions yielded marked differences between plunging jet and hydraulic jump. In the vertical plunging jet flow, the fluid entrainment into the developing shear flow caused a 90º change in momentum direction to surrounding entrained fluid. In contrast, in a hydraulic jump, the entrainment of recirculating fluid into the shear region yielded a 180º change in momentum direction. Buoyancy forces were oriented differently between the horizontal hydraulic jump and vertical plunging jet. Moreover, some substantial aeration and de-aeration took place at the free surface in the hydraulic jump.

Acknowledgments

The authors thank Dr Hang Wang (JB Pacific), Dr Matthias Kramer (The University of Queensland) and Dr Xinqian (Sophia) Leng (The University of Queensland) for helpful discussions.

References

[1] Bin, A. (1993) Gas entrainment by plunging liquid jets. *Chem. Eng. Sci.*, Vol. 48, No. 2, pp. 3585-3630.

[2] Chanson, H. (1995). Air Entrainment in Two-dimensional Turbulent Shear Flows with Partially Developed Inflow Conditions. *International Journal of Multiphase Flow*, Vol. 21, No. 6, pp. 1107-1121 (DOI: 10.1016/0301-9322(95)00048-3)

[3] Chanson, H. (1996). Air Bubble Entrainment in Turbulent Water Jets Discharging into the Atmosphere. *Australian Civil Engineering Transactions*, I.E.Aust., Vol. CE39, No. 1, Sept., pp. 39-48.

[4] Chanson, H. (1997). *Air Bubble Entrainment in Free-Surface Turbulent Shear Flows*. Academic Press, London, UK, 401 pages.

[5] Chanson, H. (2002). Air-Water Flow Measurements with Intrusive Phase-Detection Probes. Can we Improve their Interpretation ? *Journal of Hydraulic Engineering*, ASCE, Vol. 128, No. 3, pp. 252-255 (DOI: 10.1061/(ASCE)0733-9429(2002)128:3(252)).

[6] Chanson, H. (2008). Advective Diffusion of Air Bubbles in Turbulent Water Flows. in *Fluid Mechanics of Environmental Interfaces*, Taylor & Francis, Leiden, The Netherlands, C. Gualtieri and D.T. Mihailovic Editors, Chapter 7, pp. 163-196.

[7] Chanson, H. (2009a). Turbulent Air-water Flows in Hydraulic Structures: Dynamic Similarity and Scale Effects. *Environmental Fluid Mechanics*, Vol. 9, No. 2, pp. 125-142 (DOI: 10.1007/s10652-008-9078-3).

[8] Chanson, H. (2009b). Current Knowledge In Hydraulic Jumps And Related Phenomena. A Survey of Experimental Results. *European Journal of Mechanics B/Fluids*, Vol. 28, No. 2, pp. 191-210 (DOI: 10.1016/j.euromechflu.2008.06.004) (ISSN 0997-7546).

[9] Chanson, H. (2010). Convective Transport of Air Bubbles in Strong Hydraulic Jumps. *International Journal of Multiphase Flow*, Vol. 36, No. 10, pp. 798-814 (DOI: 10.1016/j.ijmultiphaseflow.2010.05.006).

[10] Chanson, H., and Brattberg, T. (2000). Experimental Study of the Air-Water Shear Flow in a Hydraulic Jump. *International Journal of Multiphase Flow*, Vol. 26, No. 4, pp. 583-607 (DOI: 10.1016/S0301-9322(99)00016-6).

[11] Cummings, P.D., and Chanson, H. (1997). Air Entrainment in the Developing Flow Region of Plunging Jets. Part 2: Experimental. *Journal of Fluids Engineering*, Transactions ASME, Vol. 119, No. 3, pp. 603-608 (DOI: 10.1115/1.2819287).

[12] Ervine, D.A. (1998). Air Entrainment in Hydraulic Structures: a Review. *Proc. Instn Civ. Engrs, Water, Maritime & Energy*, UK, Vol. 130, Sept., pp. 142-153.

[13] Goldring, B.T., Mawer, W.T., and Thomas, N. (1980). Level Surges in the Circulating Water Downshaft of Large Generating Stations. *Proc. 3rd Intl Conf. on Pressure Surges*, BHRA Fluid Eng.,F2, Canterbury, UK, pp. 279-300.

[14] Rajaratnam, N. (1965). The Hydraulic Jump as a Wall Jet. *Journal of Hydraulic Division*, ASCE, Vol. 91, No. HY5, pp. 107-132. Discussion: Vol. 92, No. HY3, pp. 110-123 & Vol. 93, No. HY1, pp. 74-76.

[15] Schlichting, H. (1979). *Boundary Layer Theory*. McGraw-Hill, New York, USA, 7th edition.

[16] Schwarz, W.H., and Cosart, W.P. (1961). The Two-Dimensional Wall-Jet. *Journal of Fluid Mechanics*, Vol.10, Part 4, pp. 481-495.

[17] Sene, K.J., Hunt, J.C.R., and Thomas, N.H. (1994). The role of coherent structures in bubble transport by turbulent shear flows. *Journal of Fluid Mechanics*, Vol. 259, pp. 219-240.

[18] Shi, R., Wang, H., and Chanson, H. (2018). Bubble Convection and Bubbly Flow Turbulent Time and Length Scales in Two-Dimensional Plunging Jets. *Experimental Thermal and Fluid Science*, Vol. 98, pp. 278-289 (DOI: 10.1016/j.expthermflusci.2018.06.008).

[19] Wang, H. (2014). Turbulence and Air Entrainment in Hydraulic Jumps. *Ph.D. thesis*, School of Civil Engineering, The University of Queensland, Brisbane, Australia, 341 pages & Digital appendices (DOI: 10.14264/uql.2014.542).

[20] Wang, H., Slamet, N.S., Zhang, G., and Chanson, H. (2018). Intrusive Measurements of Air-Water Flow Properties in Highly Turbulent Supported Plunging Jets and Effects of Inflow Jet Conditions. *Chemical Engineering Science*, Vol. 177, pp. 245-260 (DOI: 10.1016/j.ces.2017.11.030).

[21] Wood, I.R. (1991). *Air entrainment in free-surface flows*. IAHR Hydraulic structures design manual No.4, Balkema Publ., Rotterdam, The Netherlands, 149 pages.